nature methods

Matters arising

https://doi.org/10.1038/s41592-022-01694-x

Assessment of 3D MINFLUX data for quantitative structural biology in cells

Received: 5 February 2021

Accepted: 21 October 2022

Check for updates

Kirti Prakash [1,2] & Alistair P. Curd [3,4,5]

ARISING FROM: *Nature Methods* https://www.nature.com/articles/s41592-019-0688-0 (2020)

In 2017, Balzarotti et al.[1] introduced MINFLUX to localize individual fluorophores in single-molecule localization microscopy by probing the emitter with a donut-shaped excitation beam[1]. The authors attained a precision ~1 nm and resolved loci on DNA origami placed 6 nm apart. In 2020, Gwosch et al.[2] extended the method to fixed and living biological cells, and into three-dimensional (3D) localization and two colors, claiming resolutions in the range of 1–3 nm for subcellular structures[2]. Using nuclear pore complexes (NPCs) as an example, the authors measured localization precisions of 1–3 nm and asserted (1) that MINFLUX can clearly resolve the eightfold symmetry of Nup96 in single nuclear pores; (2) Nup96 is distributed along a ring of 107 nm in diameter; and (3) that 3D MINFLUX can resolve the parallel cyto- and nucleoplasmic layers of Nup96 in single pore complexes, ~50 nm apart in the axial (z) direction. However, we were not convinced by the evidence given for these claims and have therefore reanalyzed the datasets provided by the authors.

We agree with their main localization precision results, but in our reanalysis we found (1) that the eightfold symmetry of NPCs is rarely visible at a single nuclear pore level and was not clearly determined in structure-based modeling of the localization datasets; (2) that the mean or best-fit Nup96 ring diameter varies between datasets and the spread of diameters in each dataset is broader than that found by dSTORM[3]; and (3) the average z-distance between cyto- and nucleoplasmic layers of Nup96 localizations was 40.5 nm instead of ~50 nm, in the dataset on which this claim was based. Furthermore, in two-color imaging, the inner ring found in similar dSTORM experiments at 40-nm diameter[3,4] was not resolved as a ring by MINFLUX. We therefore conclude that while these MINFLUX datasets demonstrate high 3D precision in localizing molecules, they do not appear to demonstrate the accuracy of previously published state-of-the-art dSTORM imaging of NPCs[3].

Per-pore analysis

We first assessed the MINFLUX datasets by estimating the diameter of segmented Nup96 complexes (Fig. 1a–c). Qualitatively, Nup96 appeared less well sampled, comparing the number and uniformity of clusters per NPC with previous dSTORM data[3], and there was a large range of numbers of localizations per NPC (Fig. 1e). Using circle fits as described by Thevathasan et al.[3], we found the diameter distributions in the two-dimensional (2D), 3D one-color and 3D two-color datasets (Gwosch et al.[2] figs. 2a, 3f and 5c) to be 107 ± 10 nm, 108 ± 7 nm and 111 ± 5 nm (mean ± s.d., N = 20), respectively. The Nup96 ring diameter in a dataset was therefore not simply 107 nm, as stated by Gwosch et al.[2] and referenced by them in dSTORM and electron microscopy data[3,5], and it had a previously unreported spread. Our estimates for the spread of diameters (Fig. 1d) for MINFLUX data were larger than that for dSTORM data (radius 53.7 ± 2.1 nm, so diameter 107.4 ± 4.2 nm, N = 2,536)[3], and the 3D two-color MINFLUX diameters were statistically different from dSTORM results and the stated 107 nm (Methods). Gwosch et al.[6] later presented the observation of nanometer scale variability as a strength of MINFLUX, but did not explain why this variability was greater than in previous dSTORM data. We are therefore not convinced that MINFLUX outperforms dSTORM for this type of measurement and scale of a biological feature.

For two-color, 3D MINFLUX imaging of the NPC, Gwosch et al.[2] show labeled wheat germ agglutinin (WGA-CF680) residing inside the Nup96 octamer both laterally and axially. However, while dSTORM has previously resolved an inner ring of the NPC with WGA-CF680 and measured its diameter at 41 ± 7 nm with WGA-AF647 (refs. [3,4]), such structure was neither apparent in the MINFLUX data (Extended Data Fig. 1) nor discussed. Even after segmentation and closer inspection of WGA distributions, we could not visually discern a ring-like structure (Extended Data Fig. 2). Therefore, we conclude that for this particular sample, MINFLUX, unlike dSTORM, failed to resolve a ~40 nm ring structure.

Field-of-view ensemble analysis

We next analyzed the distribution of MINFLUX localizations in a field of view (FOV) using PERPL[7], a structure-based modeling technique designed for incomplete data, as is often the case for single-molecule

[1]National Physical Laboratory, Teddington, UK. [2]Integrated Pathology Unit, Centre for Molecular Pathology, The Royal Marsden Trust and Institute of Cancer Research, Sutton, UK. [3]School of Molecular and Cellular Biology, University of Leeds, Leeds, UK. [4]Centre for Computational Imaging and Simulation Technologies in Biomedicine, School of Computing, University of Leeds, Leeds, UK. [5]Pathology and Data Analytics, Leeds Institute of Medical Research at St James's, School of Medicine, University of Leeds, Leeds, UK. e-mail: kirtiprakash2.71@gmail.com; a.curd@leeds.ac.uk

https://doi.org/10.1038/s41592-022-01694-x

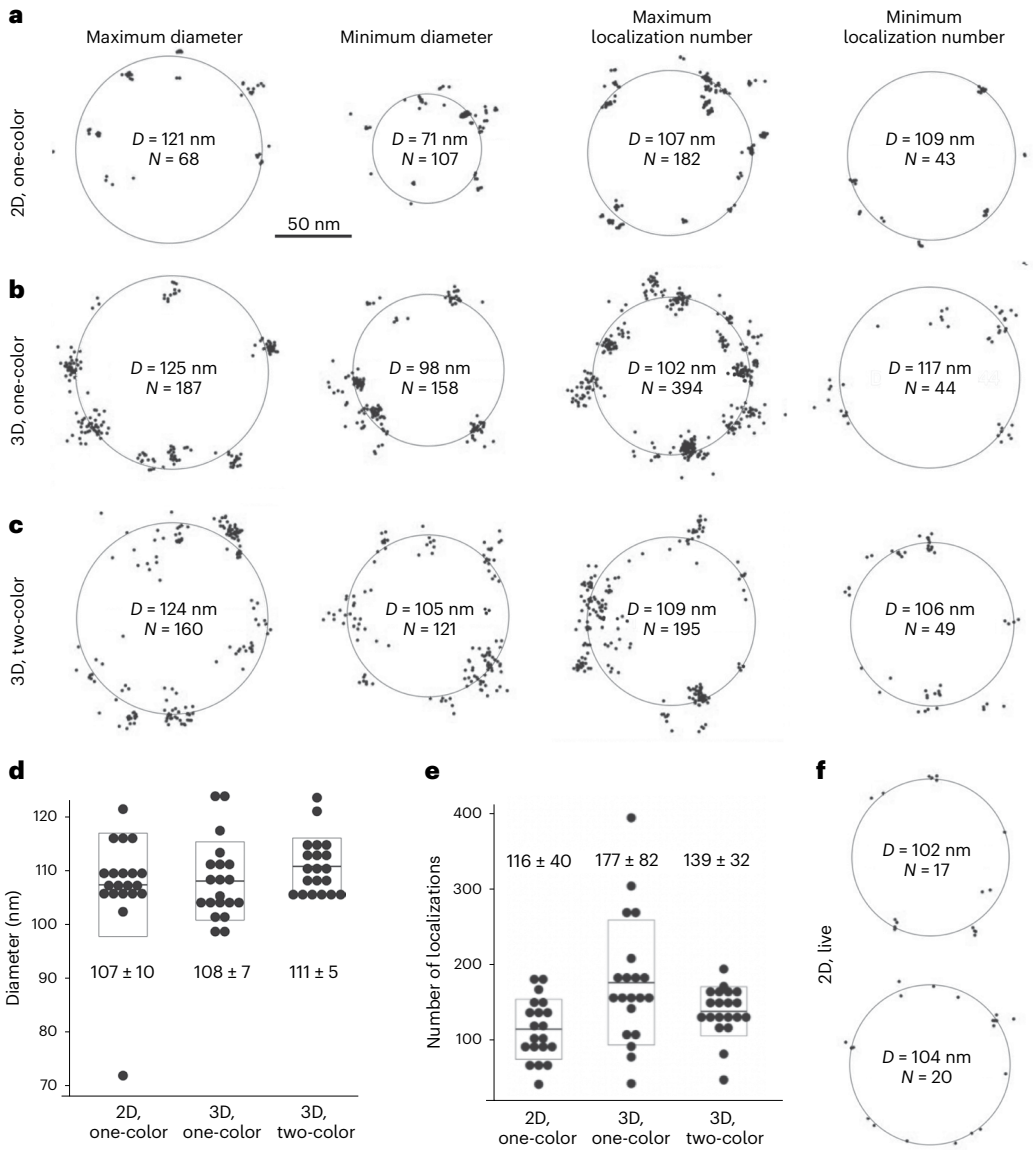

Fig. 1 | Visualization of individual nuclear pores. a–**c**,**f**, Scatter plots showing localizations from single Nup96 complexes for 2D, one-color (**a**); 3D, one-color (**b**); 3D, two-color (**c**); and 2D, live (**f**) MINFLUX datasets. **d**,**e**, Distributions of the fitted diameter (**d**) and the number of localizations (**e**) among the NPCs. Box plots show mean ± s.d., also stated. **a**–**e**, We segmented $N = 20$ NPCs for each dataset (**a**–**e**) and show those with minimum/maximum diameter and minimum/maximum number of localizations for the outer rings of Nup96 (**a**–**c**). **f**, Two Nup96 complexes were visible in the live data.

localization microscopy (SMLM)[7] (Fig. 2). Specifically, we calculated the relative position distribution of Nup96 localizations and used its components in the lateral (xy) (Fig. 2a–f) and axial (z) directions (Fig. 2g–j).

For structures in xy, a model relative position distribution that performed well for dSTORM localizations of Nup107 (ref. [7]) was fitted to the histogram of the experimental distances between MINFLUX localizations (Fig. 2a–f). Localization precision estimates (σ_{xy}) were 0.98 ± 0.02 nm, 3.20 ± 0.05 nm and 3.31 ± 0.08 nm (fitted value ± 1 s.d. uncertainty) for the 2D, 3D one-color and 3D two-color datasets, respectively, of Gwosch et al.[2], which broadly agree with the published analysis. Secondary peaks may indicate consistent substructure within clusters in the 2D dataset down to a distance of 7 nm (Fig. 2a; not modeled). However, this detail is lost in the 3D and two-color datasets (Fig. 2c,e). If σ_{xy} is in the range of 1–3 nm, we question whether the resolution is possible at 1–3 nm, as is claimed. For instance, Gaussian full width at half maximum (FWHM) ≈ 2.355σ, so σ_{xy} of 1–3 nm implies FWHM of 2.4–7.1 nm for a single molecule, and we would not expect to resolve molecules closer than this clearly.

Estimates of the Nup96 ring diameters varied from 104 to 109 nm and orders of symmetry from seven- to ninefold, for the different datasets (Fig. 2a–f and Extended Data Table 1). The best fits do not follow the experimental distance distribution as closely as for Nup107 dSTORM data[7], which may be due to the effect of intra-cluster substructure (Fig. 2a,b), a more variable arrangement of Nup96, or a smaller number of NPCs and localizations in the FOV. In particular, filtering out a larger fraction of localizations (Extended Data Fig. 3) appears to have caused the background to deviate from linear (Fig. 2a,b) to a more complex distribution (Fig. 2c–f). These analyses are not consistent with the claim that MINFLUX obtains a diameter of exactly 107 nm and eightfold symmetry, as reported by Gwosch et al.[2], who did not perform any structural analysis in xy. Such conclusive results may be difficult to obtain from these datasets, with small numbers of NPCs (N ~ 20–30, including incomplete complexes), and larger datasets would be useful to establish them.

In the axial (z) direction, using PERPL (Fig. 2g–j), we estimated localization precision (σ_z) at 2.28 ± 0.05 nm and 3.08 ± 0.06 nm for

https://doi.org/10.1038/s41592-022-01694-x

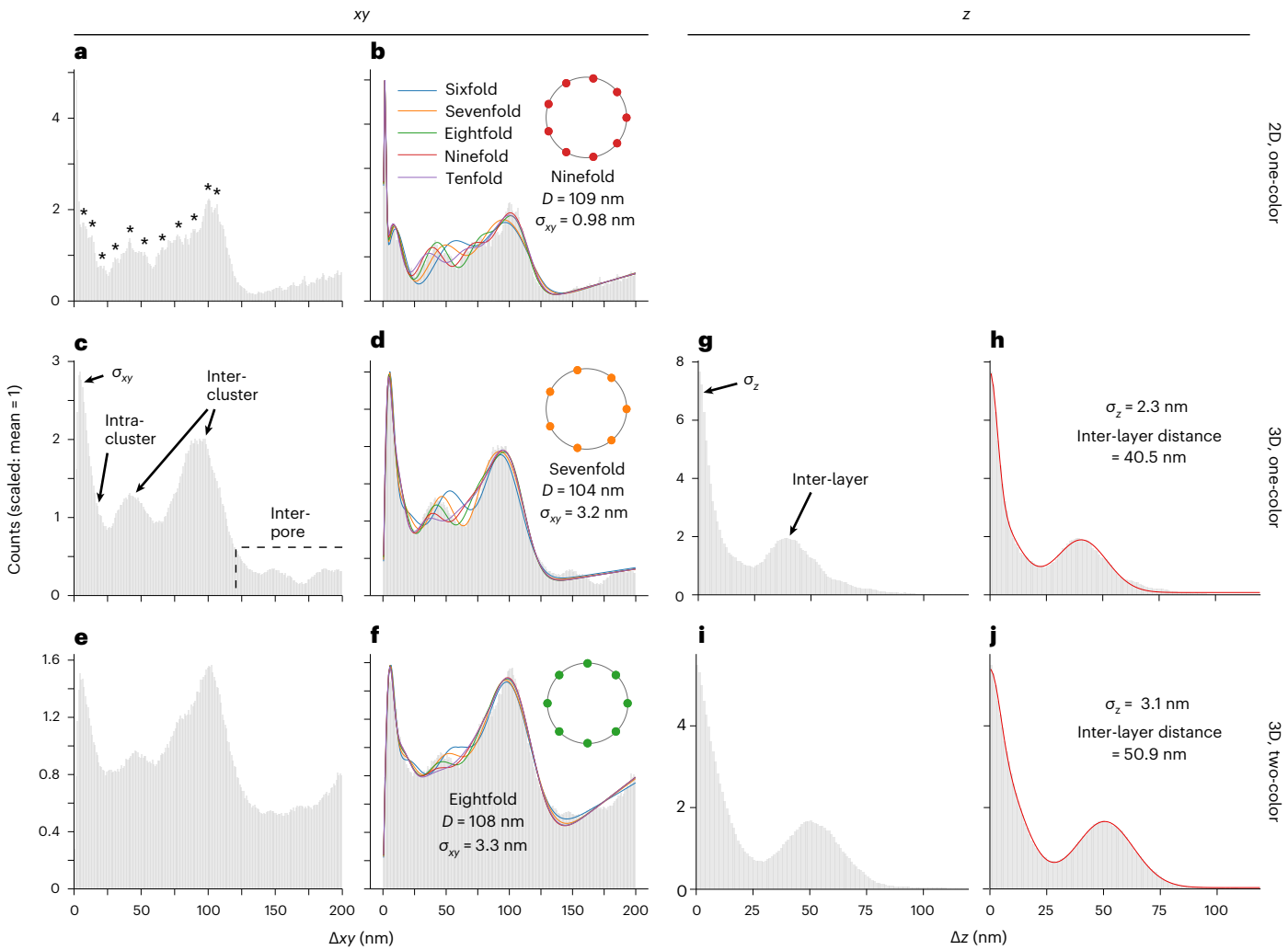

Fig. 2 | Relative position distributions and model analysis. Histograms of *xy*- and *z*-distances (Δ*xy*, Δ*z*) between localizations, bin-width 1 nm. Counts scaled to a mean of 1 to optimize the performance of the fitting algorithm. Δ*xy* distribution for the Nup96 localizations of Gwosch et al.[2] figs. 2a (**a**), 3f (**c**) and 5c (**e**) and fits to them (**b**,**d**,**f**) of nuclear porin models from six- to tenfold symmetry, including repeated single-molecule localizations (Δ*xy*), intra- and inter-cluster distances within an NPC, and background ~ inter-pore distances[7]. Symmetry, nuclear pore diameter (*D*) and σ_{xy} for the model selected by AICc[7] in each experiment (**b**,**d**,**f**). Indications of resolved intra-cluster substructure in **a** (*). Δ*z* distribution for the data in Gwosch et al.[2] figs. 3f (**g**) and 5c (**i**) and fit with a model including two layers of localizations and repeated single-molecule localizations (σ_z) (**h**,**j**).

the 3D, one-color and two-color datasets of Gwosch et al.[2], demonstrating the high localization precision in *z*, and implying that best possible resolution in $z \approx 5–7$ nm (FWHM). For the 3D one-color dataset of Gwosch et al.[2] fig. 3f, we found the distance between the Nup96 layers to be 40.5 ± 0.2 nm (Fig. 2g,h), and not ~50 nm, as claimed by Gwosch et al. (no quantitative analysis provided)[2] and previously obtained in dSTORM[3]. By contrast, in the two-color dataset of Gwosch et al.[2] fig. 5c, we estimated the inter-layer distance at 50.89 ± 0.08 nm (Fig. 2i,j), close to the expected ~50 nm (and estimated at ~46 nm by Gwosch et al.). We also verified that the different results from the data of Gwosch et al.[2] figs. 3f and 5c were not explainable by a difference in nuclear envelope inclination or local NPC tilt (Extended Data Fig. 4 and Supplementary Videos 1 and 2); we agree with Gwosch et al.[2], who noted that the NPC layers were typically parallel to the focal plane. Gwosch et al.[6] have later explained this difference by disagreeing both with their original publication on this point[2] and with modeling and 3D visualization of the data (Extended Data Fig. 4 and Supplementary Videos 1 and 2). Thus, we were not convinced that MINFLUX provides accurate quantitative measures in the axial direction.

Localization probability, live-cell results

We reproduced the published images of Gwosch et al.[2] and noted that localization densities are low (~450–1,200 µm^{-2}; Extended Data Fig. 3a–c), compared with representative regions in dSTORM on the same sample type with the same labeling method (~2,600–3,450 µm^{-2}, Extended Data Fig. 5; Thevathasan et al.[3]). Fewer data points, meaning reduced signal, are therefore available for structural resolution. We also note that a lower probability of target molecules being localized results in increased noise in structural information, from false negatives in localizing real features in the structure. These effects on the signal-to-noise ratio may be the reason for structures appearing less clear and for differences in quantitative results and their uncertainties, despite very high localization precisions, as noted. Additionally, this may explain the higher accuracy of the inter-layer distance for the data with higher localization density (Fig. 2h,j and Extended Data Fig. 3b,c).

The lowest localization density was obtained for live-cell data, as is often the case in SMLM. With $N = 2$ NPCs and 38 localizations (Extended Data Fig. 3d; Gwosch et al.[2] fig. 2f), there was too little data available to assess the claim of resolution at 1–3 nm in living cells. Circular fits found diameters of 102 nm and 104 nm (Fig. 1f; ideal result 107 nm).

We are therefore unable to quantitatively assess σ_{xy}, resolution and reliability in this case, since we could not use PERPL analysis on only two instances of the NPC with missing data.

Furthermore, Gwosch et al.[2] did not calculate localization precision in the live sample. In a fixed sample, they measured σ_{xy} ~ 2 nm for the same label, Nup96-mMaple (Gwosch et al.[2] Supplementary fig. 7), which gives a possible resolution limit (i.e. FWHM) of ~5 nm in that case. However, precision and resolution are generally degraded when moving from fixed to live specimens, so we do not expect nanometer (1–3 nm) resolution in the case of live MINFLUX imaging, on the basis of these datasets.

Discussion

From our reanalysis of the data reported by Gwosch et al.[2], we were unable to confirm that MINFLUX delivers 3D multicolor nanometer resolution (1–3 nm) for structures in fixed and living cells, at the current stage of the technology. In fact, it generated less precise and reliable results than established SMLM methods and appeared unable to resolve a 40-nm ring structure, despite using the same sample and comparable labeling methods to those in previous dSTORM data[2,3].

After event filtering, 3D Nup96-AF647 localization precision in fixed samples is impressive at $\sigma = 1–3$ nm. However, we advise against interpreting localization precision (σ) as resolution, which is intuitively understood as the minimum distance separating two nearby features at which they can be distinguished. Resolution is worse than 2σ at a lower limit and is affected by other factors such as localization density, or the probability of localizing target molecules. We note that methods that increase localization precision may also reduce localization probability (including event filtering) and thus worsen resolution. This merits further exploration when resolving structural information is the goal, in this and other SMLM methods. We suggest assessing resolution, detection efficiency and exploration of event filtering algorithms on blind samples, to demonstrate the potential of this new technology. For an initial discussion of these issues, see Prakash[8].

We fully expect MINFLUX methods to continue to improve, as they have done in the powerful iterative and 3D developments already reported[2]. However, we recommend that experimentalists also perform initial testing of the resolution, detection efficiency and exploration of event filtering algorithms on potential samples, to the extent this is possible, before choosing MINFLUX over other SMLM techniques.

Online content

Any methods, additional references, Nature Portfolio reporting summaries, source data, extended data, supplementary information, acknowledgements, peer review information; details of author contributions and competing interests; and statements of data and code availability are available at https://doi.org/10.1038/s41592-022-01694-x.

References

1. Balzarotti, F. et al. Nanometer resolution imaging and tracking of fluorescent molecules with minimal photon fluxes. *Science* **355**, 606–612 (2017).
2. Gwosch, K. C. et al. Minflux nanoscopy delivers 3D multicolor nanometer resolution in cells. *Nat. Methods* **17**, 217–224 (2020).
3. Thevathasan, J. V. et al. Nuclear pores as versatile reference standards for quantitative superresolution microscopy. *Nat. Methods* **16**, 1045–1053 (2019).
4. Löschberger, A. et al. Super-resolution imaging visualizes the eightfold symmetry of gp210 proteins around the nuclear pore complex and resolves the central channel with nanometer resolution. *J. Cell Sci.* **125**, 570–575 (2012).
5. Von Appen, A. et al. In situ structural analysis of the human nuclear pore complex. *Nature* **526**, 140–143 (2015).
6. Gwosch, K. et al. Assessment of 3D MINFLUX data for quantitative structural biology in cells revisited. Preprint at *bioRxiv* https://doi.org/10.1101/2022.05.13.491065 (2022).
7. Curd, A. P. et al. Nanoscale pattern extraction from relative positions of sparse 3D localizations. *Nano Lett.* **21**, 1213–1220 (2021).
8. Prakash, K. At the molecular resolution with MINFLUX? *Philos. Trans. R. Soc. A* **380**, 20200145 (2022).

Methods

In per-pore analysis (Fig. 1), we used the MATLAB function circlefit (https://uk.mathworks.com/matlabcentral/fileexchange/5557-circle-fit) to fit a circle to a set of (x, y) points.

Statistical analysis of 3D two-color MINFLUX diameters of Nup96 rings, compared with reference results[3,5], used the stats module within the Python library scipy 1.3 (ref. [9]). The distribution of the 20 MINFLUX diameters was tested for normality[10,11] and accepted (stats.normaltest, $P = 0.13$). The mean ± s.d. of the 3D two-color diameters is 110.7 ± 5.2 nm ($N = 20$). The mean MINFLUX diameter was statistically different from 107 nm (quoted from electron microscopy data by Gwosch et al.[2]) (one-sample t-test, two-tailed: $t = 3.159$, $P = 0.005$), using the 20 measured diameter values. The mean MINFLUX diameter was also significantly different from the previous dSTORM result on Nup96 ring diameters with the same sample and comparable labeling methods[2,3] (107.4 ± 4.2 nm, $N = 2{,}536$)[3] (Welch's unequal variances t-test, two-tailed: $t = 2.888$, $P = 0.009$), using the sample means and standard deviations.

FOV ensemble analysis (Fig. 2 and Extended Data Fig. 4) used PERPL[7] 0.12 m (https://bitbucket.org/apcurd/perpl-python3/commits/tag/0.12m). The xy-model includes Gaussian clusters arranged symmetrically around a ring, repeated localizations of a single molecule (with s.d. spread σ_{xy}), and a linearly increasing background term. The z-model includes two layers of localizations, each with a Gaussian distribution in z, a term for localization precision (σ_z) for repeated localizations of a single molecule, and constant background.

Nup96 structural model selection (Fig. 2 and Extended Data Table 1) used the corrected Akaike's Information Criterion (AICc)[12], as in Curd et al.[7], from the residuals of the model fits. In brief, lower AICc values among compared models indicate quantitatively that less information from the real data distribution is lost when the fitted models are used to approximate the real data. Lower AICc thus results in higher relative likelihoods among compared models. The AICc is a relative value among models being compared, not an absolute value, and cannot be compared across different datasets (for example results for 2D, one-color can be compared with each other, but not with results for 3D, one-color). As a guide, if AICc differs by six between models, one is 20 times more likely to be the best model than the other (ratio: $\exp\left(-\frac{1}{2}\Delta\mathrm{AICc}\right)$)[12].

Localization density (Extended Data Figs. 3 and 5) was calculated as the number of MINFLUX events labeled as true localizations, divided by the area of the FOV as defined by the ranges in x and y of all localizations before filtering.

Reporting summary

Further information on research design is available in the Nature Portfolio Reporting Summary linked to this article.

Data availability

The original MINFLUX data[2] was made available by S. Hell. All the reanalyzed data has been deposited to Zenodo at https://doi.org/10.5281/zenodo.5214631. Source data are provided with this paper.

Code availability

Plots for Fig. 2 and Extended Data Fig. 4 were generated using PERPL[7] 0.12m, available at https://bitbucket.org/apcurd/perpl-python3/commits/tag/0.12m.

References

9. Virtanen, P. et al. SciPy 1.0: fundamental algorithms for scientific computing in Python. *Nat. Methods* **17**, 261–272 (2020).
10. D'Agostino, R. B. An omnibus test of normality for moderate and large size samples. *Biometrika* **58**, 341–348 (1971).
11. D'Agostino, R. & Pearson, E. S. Tests for departure from normality. Empirical results for the distributions of b^2 and $\sqrt{b}^1$. *Biometrika* **60**, 613–622 (1973).
12. Burnham, K. P. & Anderson, D. R. *Model Selection and Inference: A Practical Information-Theoretic Approach* 75–117 (Springer, New York, 1998).
13. Heydarian, H. et al. 3D particle averaging and detection of macromolecular symmetry in localization microscopy. *Nat. Commun.* **12**, 2847 (2021).

Acknowledgements

All analysis was done on MINFLUX localization data provided by the Hell lab in tabular format (Extended Data Table 2). We would like to thank L. Schermelleh, J. Hohlbein, M. Peckham and P. Knight for helpful discussions. A.P.C. gratefully acknowledges funding by the UK Biotechnology and Biological Sciences Research Council (BB/S015787/1) and ~~the Wellcome Institutional Strategic Support Fund (University of Leeds)~~.

Author contributions

K.P. conceived the project. K.P. and A.P.C. designed the project, performed data analysis, interpreted results and wrote the manuscript.

Competing interests

The authors declare no competing interests.

Additional information

Extended data is available for this paper at https://doi.org/10.1038/s41592-022-01694-x.

Supplementary information The online version contains supplementary material available at https://doi.org/10.1038/s41592-022-01694-x.

Correspondence and requests for materials should be addressed to Kirti Prakash or Alistair P. Curd.

Peer review information *Nature Methods* thanks Bernd Rieger and the other, anonymous, reviewers for their contribution to the peer review of this work. Primary Handling editor: Rita Strack, in collaboration with the *Nature Methods* team.

https://doi.org/10.1038/s41592-022-01694-x

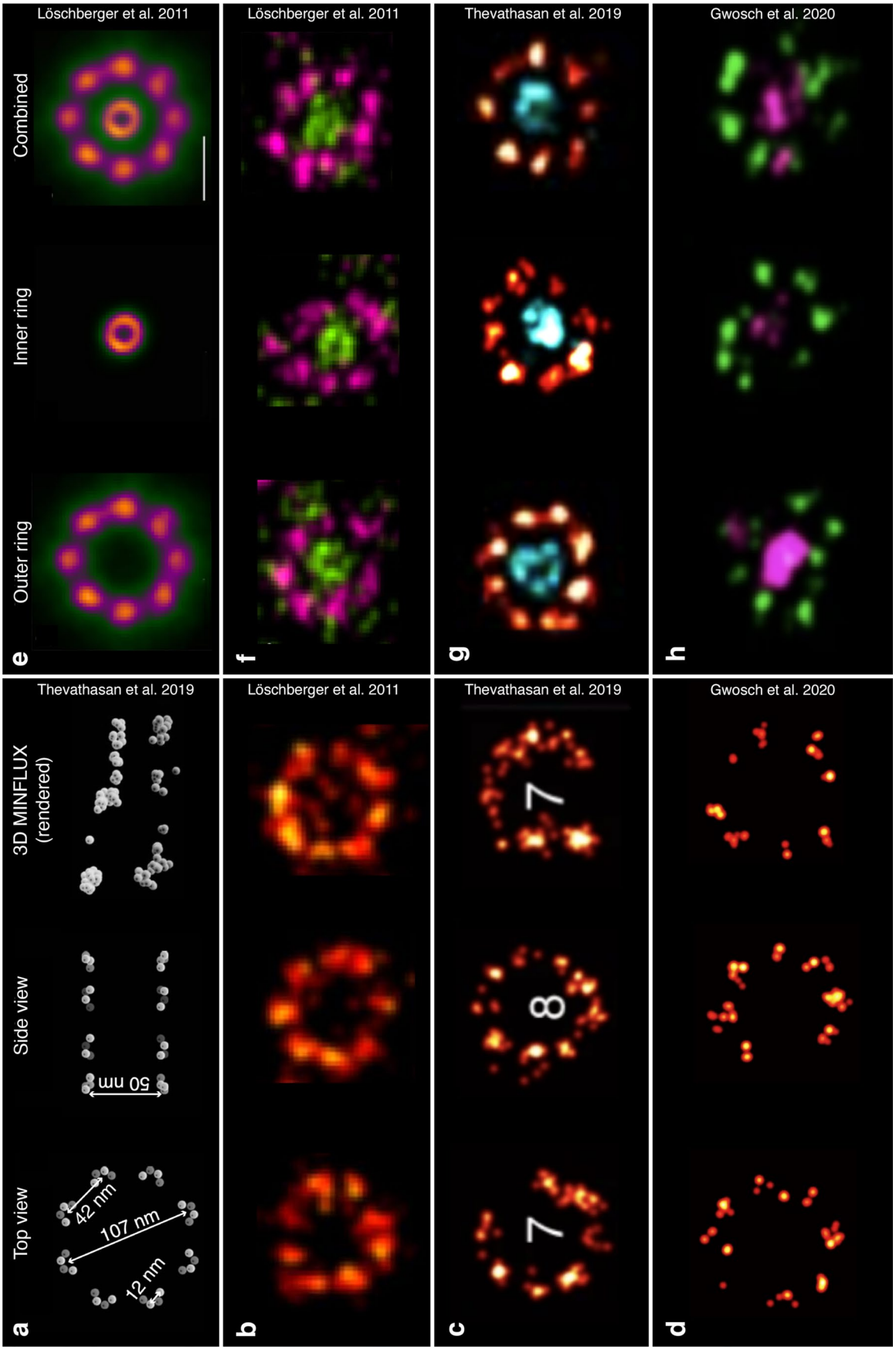

Extended Data Fig. 1 | See next page for caption.

https://doi.org/10.1038/s41592-022-01694-x

Extended Data Fig. 1 | Nuclear pores across different imaging modalities. (**a**) A schematic of the Nup96 complex, taken from Thevathasan et al.[3]. 3D MINFLUX rendered data presented for comparison from Gwosch et al.[2] (colormap removed for comparison). Note the uneven distribution in *xz*, compared with the EM model (Von Appen et al.[5] and dSTORM data in Thevathasan et al.[3] fig. 2h. (**b**) Membrane protein gp210 from amphibian oocytes imaged with dSTORM (Alexa Fluor 647). The 8-fold symmetry and circular structure of NPCs are generally seen. The diameter of gp210 is 164 ± 7 nm. Image adapted from Loeschberger et al.[4]. (**c**) Nup96 endogenously labeled with SNAP-tag-Alexa Fluor 647 in U2OS cell lines. 8- and 7-component pores are more commonly observed. The effective labeling efficiency for SNAP-Alexa Fluor 647 was ~60%. Image adapted from Thevathasan et al.[3]. (**d**) MINFLUX imaging of U2OS cell expressing Nup96–SNAP labeled with Alexa Fluor 647. In this dataset (Gwosch et al.[2] fig. 2a), 6- and 7-component nuclear pores are more prominent throughout the FOV, raising a question about detection efficiency. Localizations were rendered with a Gaussian kernel, σ = 2 nm, to visualize the 4 individual copies of Nup96 per NPC subunit (1–5 sub-clusters per subunit apparent here). In multicolor MINFLUX imaging, the localizations in a subunit appear as a larger, undefined cluster (**h**). Cell line and labeling strategy as in Thevathasan et al.[3]. Image adapted from Gwosch et al.[2]. (**e**) Average images of gp210 (outer ring, $N = 426$) and WGA (central channel, $N = 621$) of the NPC. The outer ring (gp210) has an average diameter of ~164 nm. The diameter of the inner ring (WGA) is ~40 nm. Image adapted from Loeschberger et al.[4]. Scale bar: 100 nm. (**f**) dSTORM images of WGA labeled with ATTO 520 (green) and gp210 labeled with Alexa Fluor 647 (pink) in amphibian oocytes. Both the outer ring and inner channel are visible (Loeschberger et al.[4]). (**g**) Two-color SMLM image of Nup96–SNAP-Alexa Fluor 647 (red) and WGA-CF680 (cyan) in U2OS cell lines. The outer ring is clearly visible and the inner ring is also visible in most cases. Image adapted from Thevathasan et al.[3]. (**h**) Two-color MINFLUX imaging of U2OS cell expressing Nup96–SNAP labeled with Alexa Fluor 647 and WGA conjugated to CF680. The subunits of the outer ring, which each have 4 copies of Nup96, now appear as single clusters (comparing with **c**). The inner ring (WGA) also appears as undefined aggregations of the signal. Image adapted from Gwosch et al.[2].

https://doi.org/10.1038/s41592-022-01694-x

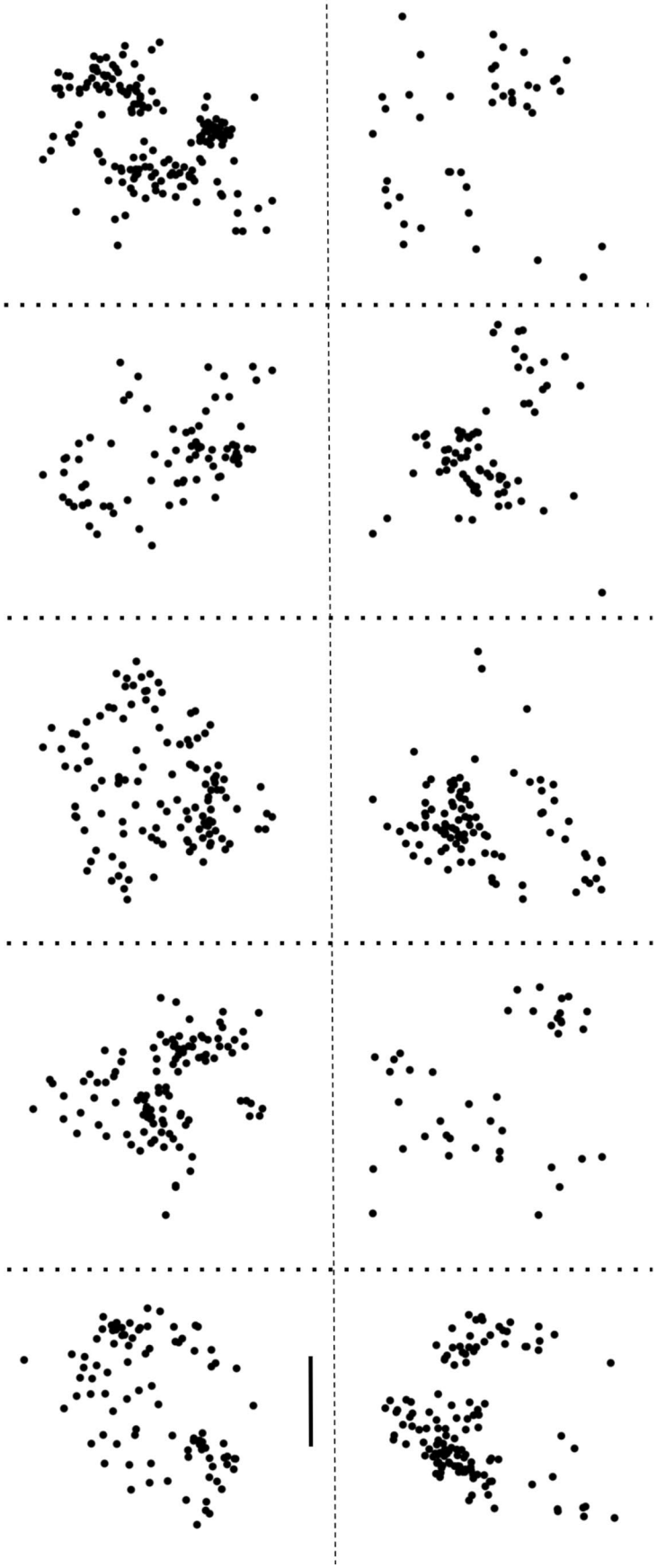

Extended Data Fig. 2 | Visualization of the inner ring of nuclear pores (wheat germ agglutinin (WGA). Scatter plots showing localizations from 10 segmented WGA complexes from the 3D, 2-color MINFLUX dataset. The segmented complexes did not contain rings of localizations as found by Thevathasan et al.[3] and Loeschberger et al.[4] Scale bar: 20 nm.

https://doi.org/10.1038/s41592-022-01694-x

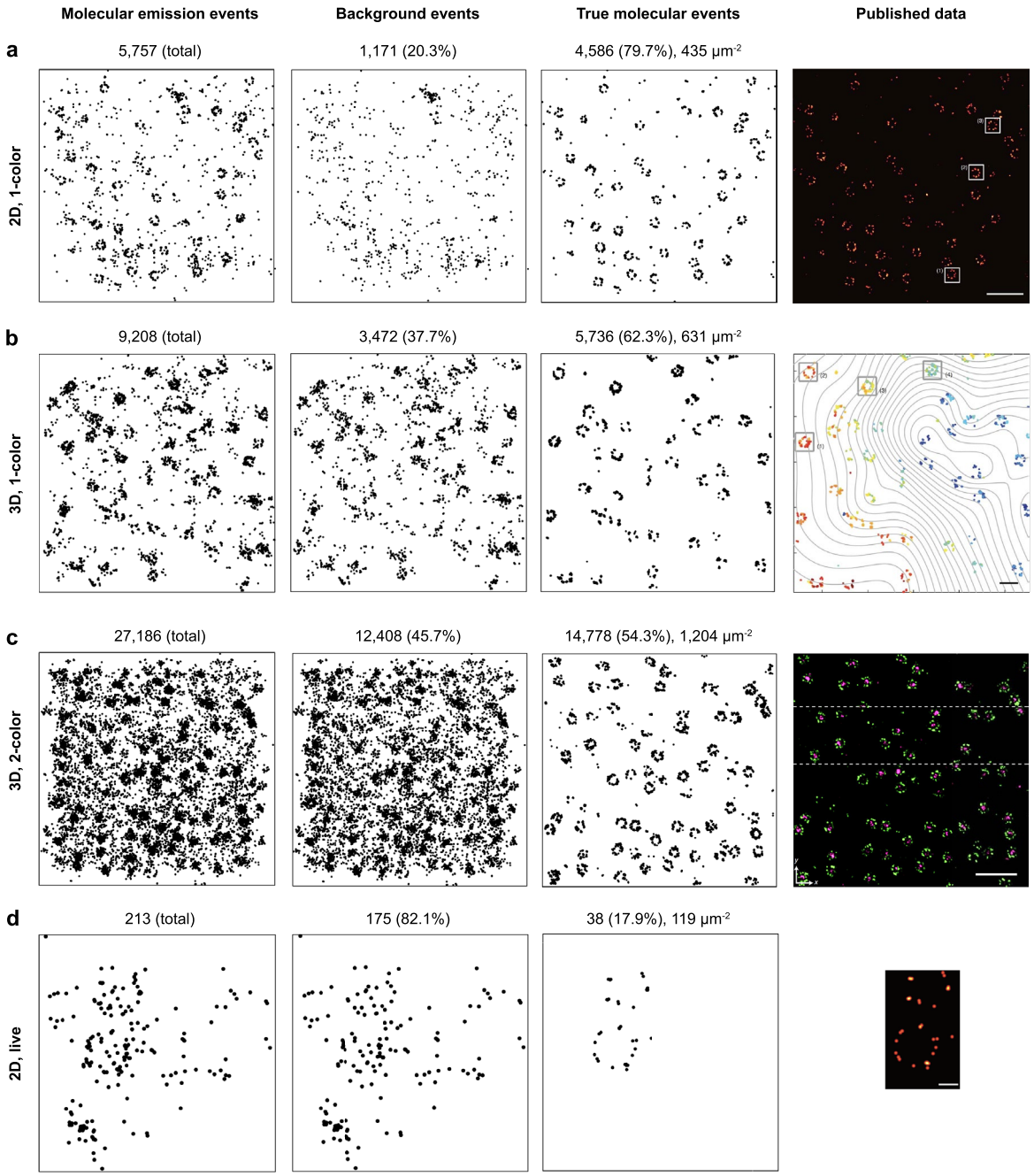

Extended Data Fig. 3 | MINFLUX localization filtering. Scatter plots for 2D, 1-color (**a**); 3D, 1-color (**b**); 3D, 2-color (**c**); and 2D, live (**d**) unfiltered and filtered MINFLUX datasets. The raw MINFLUX data comes in a tabular format, with a Boolean flag indicating that localization was assigned as either a background event or a true molecular event (Gwosch et al.[2], Extended Data Table 2). For the final data, we give the density of true localizations over the FOV defined by the total molecular emission events before filtering. Scale bar: 500 nm (a), 200 nm (b), 500 nm (c), 50 nm (d) in the published data column.

https://doi.org/10.1038/s41592-022-01694-x

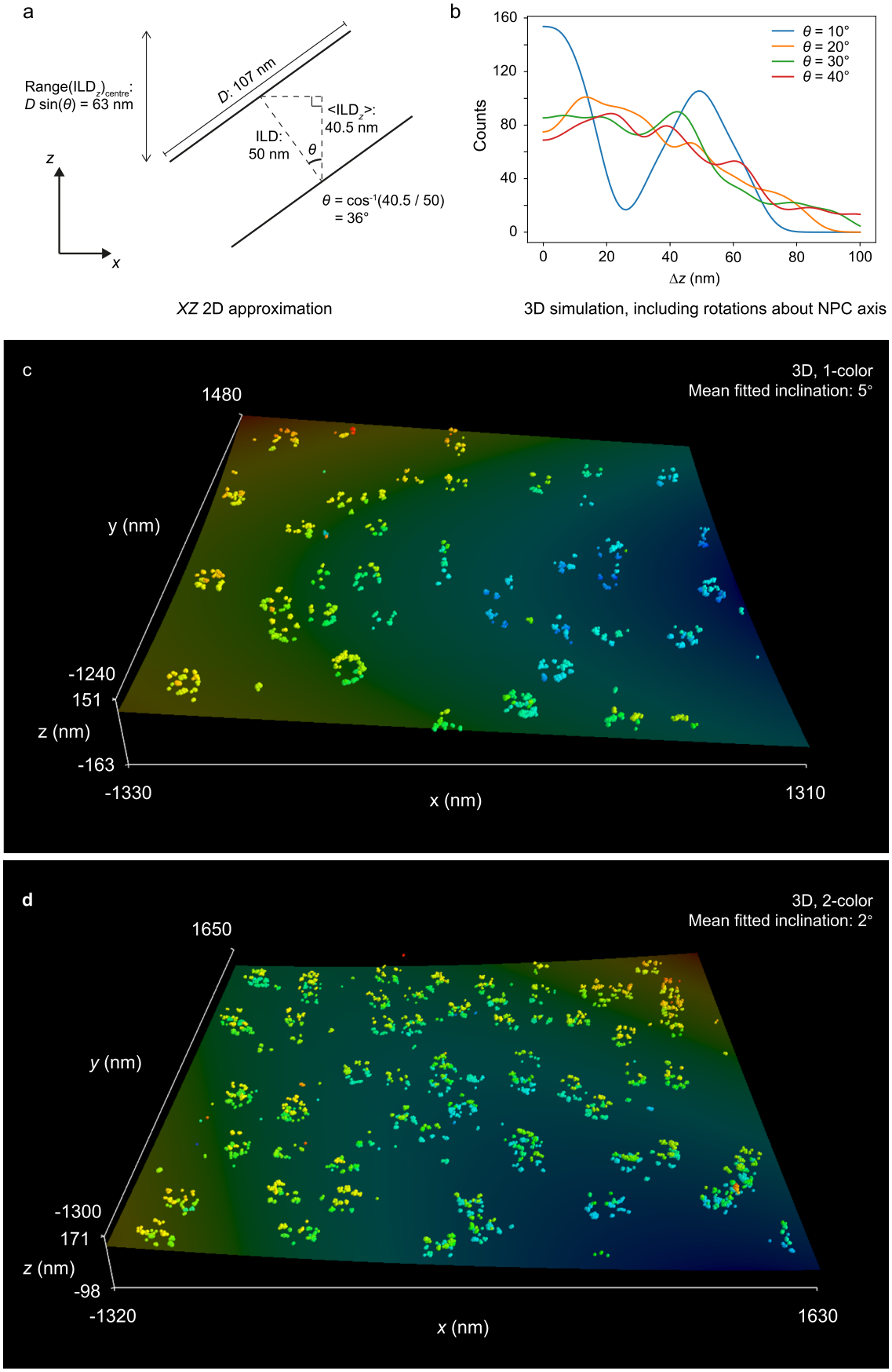

Extended Data Fig. 4 | See next page for caption.

https://doi.org/10.1038/s41592-022-01694-x

Extended Data Fig. 4 | NPC tilt and *z*-distances. A 2D projection model of the two-layer NPC (**a**) requires its axis to be tilted (θ) by 36° for an inter-layer distance (ILD) of 50 nm between localizations to result in an average measurement in the *z*-direction (<ILD_z>) of 40.5 nm. Considering *z*-measurements only from the center point of the lower layer to all points on the upper layer, ILD_z has a range (Range$(ILD_z)_{center}$) of 63 nm, when the diameter (*D*) of the projected NPC is 107 nm. Including *z*-measurements from all points in the lower layer to all points on the upper layer doubles the total range of ILD_z to 125 nm, which is large compared with <ILD_z>. Therefore if localizations with ILD of 50 nm were measured to have <ILD_z> of 40.5 nm, we would expect the NPCs to be tilted to ~36° and also expect *z*-measurements between the layers to have a broad spread, before considering additional spread owing to a distribution of NPC tilt angles. Distributions of Δz between localizations in a 3D NPC model (**b**) show a similar pattern. The NPC model used localizations with a two-layer, 8-fold radially symmetric structure, with an inter-layer distance of 50 nm and diameter of 107 nm. At each value of θ (tilt of the model axis from the *z*-direction), the model was also rotated about its axis by angles φ from 0 to 44° in 1° increments. Δz values were found between all localizations at each rotation angle φ and aggregated over φ to result in an averaged distribution at each tilt angle θ. In agreement with the 2D model (**a**), the inter-layer distance peak moved to shorter distances for higher tilt angles θ, approaching 40 nm between $\theta = 30°$ and $\theta = 40°$. The inter-layer distance peak was still close to 50 nm at $\theta = 10°$. In further agreement with **a**, and as may be intuitively expected, broadening of the Δz distribution with increasing θ significantly reduced the contrast of the inter-layer distance peak for $\theta \geq 20°$. Therefore, it is highly unlikely that the high-contrast peak at 40.5 nm (Fig. 2g,h) of the experimental Δz distribution of the data of Gwosch et al.[2] fig. 3f would be generated by two layers of localizations with an inter-layer distance of 50 nm, tilted at 30–40°. Rather, we support the statement of Gwosch et al. that the layers of the NPCs in Gwosch et al.[2] were typically parallel to the focal plane. We also support this statement as a reasonable approximation in a 3D scatter plot of the localizations (**c**, Supplementary Video 1) of Gwosch et al.[2] fig. 3f. In this plot, NPC layers, when discernible, appear generally to be roughly parallel to a fitted surface representing nuclear envelope curvature (quadratic in *x* and *y*, fitted to the localization coordinates). The mean inclination of this surface at the localization coordinates is 5° (maximum: 9°). At $\theta = 5°$, an ILD of 50 nm would result in <ILD_z> of 49.8 nm (**a**), or a fractional difference of 0.4% between ILD and <ILD_z>. A narrow distribution of local NPC tilts with a peak at this angle may be expected (for example s.d. 12° in Heydarian et al.[13]). Our result in Fig. 2g,h, therefore, reflects the inter-layer distance of the acquired localizations, not a projection of a two-layer structure at large tilt angles. Furthermore, a similar 3D plot and fit (**d**, Supplementary Video 2) of the Nup96 localizations of Gwosch et al.[2] fig. 5c shows a similar (but denser) distribution of NPCs. In this case, the mean fitted nuclear envelope inclination was 2° (maximum: 5°), and we also expect NPCs to have a similar distribution of local tilt angles centered on this angle[13]. In this case, we found an inter-layer distance of 50.9 nm (Fig. 2i,j), which is in fact greater than the calculation of Gwosch et al.[2] at ~46 nm, despite the similar NPC tilts between the two datasets. From these considerations (**a**–**d**), the difference between our inter-layer distance results of 40.5 nm and 50.9 nm for the two datasets are not explained by a difference in NPC tilts.

https://doi.org/10.1038/s41592-022-01694-x

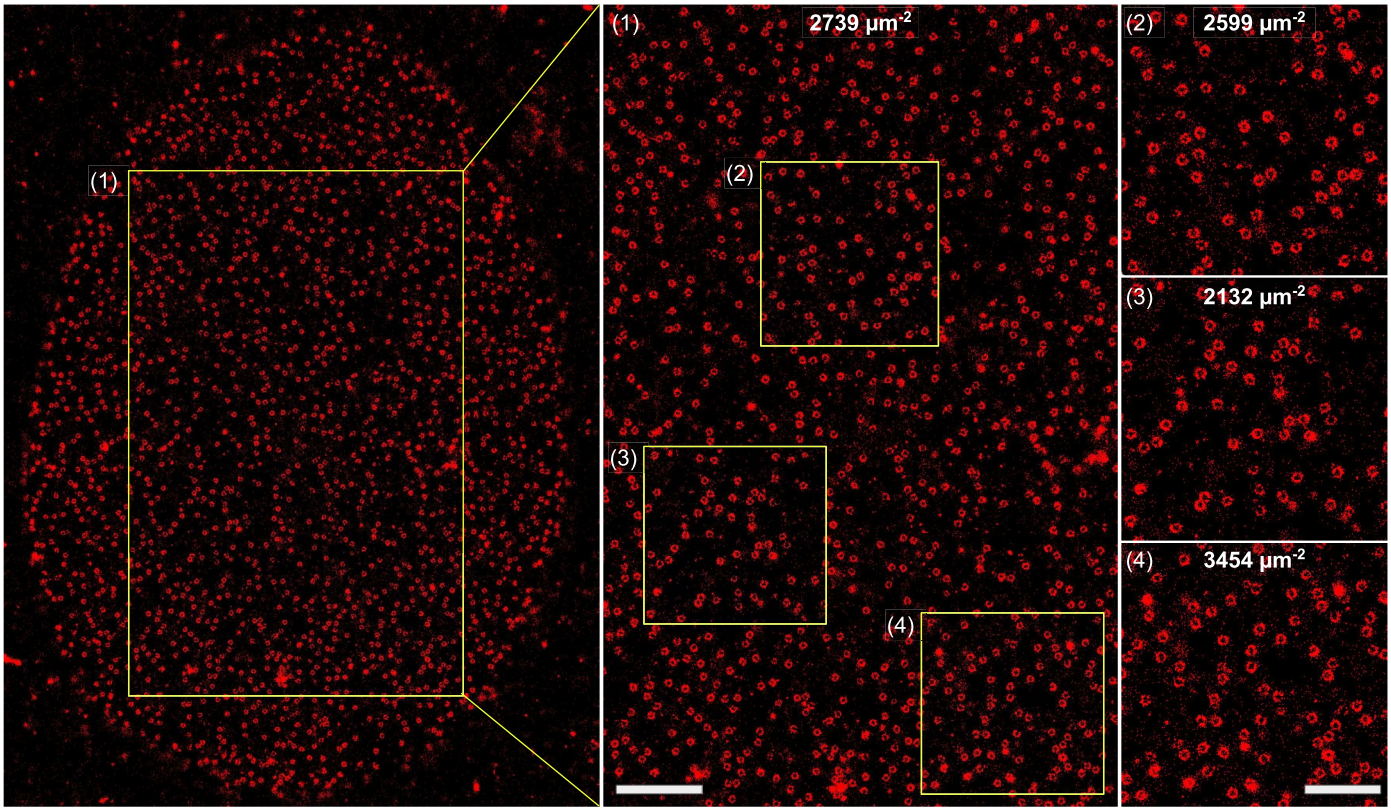

Extended Data Fig. 5 | dSTORM localization density from Thevathasan et al.[3]**.** From publicly available data (https://www.ebi.ac.uk/biostudies/BioImages/studies/S-BIAD8), localization densities were calculated over the nuclear regions shown. Compared to 2D, 1-color MINFLUX data (Fig. 3) which has an average localization density of 435 μm^{-2}, 2D, 1-color dSTORM has a ~6x greater average localization density of 2739 μm^{-2}. Scale bar: 3 μm in (1) and 1 μm in (2), (3), (4).

https://doi.org/10.1038/s41592-022-01694-x

Extended Data Table 1 | Corrected Akaike Information Criterion values (AICc) and relative likelihoods for different symmetric models fitted to the Δ*xy* distributions of Fig. 2

	2D, 1-color		3D, 1-color		3D, 2-color	
	AICc	Relative likelihood	AICc	Relative likelihood	AICc	Relative likelihood
6-fold	−564.92	<0.01	−768.43	<0.01	−1114.98	<0.01
7-fold	−648.93	<0.01	−988.03	1	−1149.43	<0.01
8-fold	−816.15	<0.01	−945.01	<0.01	−1171.03	1
9-fold	−877.36	1	−876.87	<0.01	−1154.44	<0.01
10-fold	−801.00	<0.01	−859.74	<0.01	−1138.56	<0.01

AICc and relative likelihoods for each model to be the best model were calculated as for Nup107 distributions in Curd et al.[7].

https://doi.org/10.1038/s41592-022-01694-x

Extended Data Table 2 | MINFLUX dataset (localization positions and filtering data) as provided by the authors (Gwosch et al.[2])

	x_est_absolute	y_est_absolute	N [double]	p0 [double]	r_relative	Filter	molecularID
1	571.23	1246.22	3401	0.07	0	1	1
2	569.37	1245.37	2003	0.07	0.01	1	2
3	570.61	1243.29	1999	0.06	0.01	1	2
4	570.77	1244.45	2000	0.07	0.01	1	2
5	571.49	1244.61	3905	0.07	0.01	1	2
6	571.61	1245.34	2912	0.06	0.01	1	2
7	569.73	1243.96	3570	0.05	0	1	3
8	-569.06	-200.72	2001	0.26	0.02	0	4
9	-567.14	-199.52	2001	0.25	0.03	0	4
10	-568.3	-200.28	2188	0.25	0.03	0	4

x_est_absolute[double]: Absolute estimated molecule position in um. y_est_absolute [double]: Absolute estimated molecule position in um. N [double]: Number of photons used for localization. p0 [double]: Ratio of photons collected for central STC position. r_relative [double]: Relative distance of molecule position with respect to the central STC position in um. filter [logical] (1-color data only): Boolean flag result of event filters. True: localization is valid (molecular emission event). False: localization is invalid (background event). moleculeID [double]: ID of molecular emission event.

nature portfolio

Corresponding author(s): Kirti Prakash and Alistair P. Curd

Last updated by author(s): Aug 23, 2022

Reporting Summary

Nature Portfolio wishes to improve the reproducibility of the work that we publish. This form provides structure for consistency and transparency in reporting. For further information on Nature Portfolio policies, see our Editorial Policies and the Editorial Policy Checklist.

Statistics

For all statistical analyses, confirm that the following items are present in the figure legend, table legend, main text, or Methods section.

n/a	Confirmed	
☐	☒	The exact sample size (*n*) for each experimental group/condition, given as a discrete number and unit of measurement
☐	☒	A statement on whether measurements were taken from distinct samples or whether the same sample was measured repeatedly
☒	☐	The statistical test(s) used AND whether they are one- or two-sided *Only common tests should be described solely by name; describe more complex techniques in the Methods section.*
☒	☐	A description of all covariates tested
☒	☐	A description of any assumptions or corrections, such as tests of normality and adjustment for multiple comparisons
☐	☒	A full description of the statistical parameters including central tendency (e.g. means) or other basic estimates (e.g. regression coefficient) AND variation (e.g. standard deviation) or associated estimates of uncertainty (e.g. confidence intervals)
☐	☒	For null hypothesis testing, the test statistic (e.g. *F*, *t*, *r*) with confidence intervals, effect sizes, degrees of freedom and *P* value noted *Give P values as exact values whenever suitable.*
☒	☐	For Bayesian analysis, information on the choice of priors and Markov chain Monte Carlo settings
☒	☐	For hierarchical and complex designs, identification of the appropriate level for tests and full reporting of outcomes
☒	☐	Estimates of effect sizes (e.g. Cohen's *d*, Pearson's *r*), indicating how they were calculated

Our web collection on statistics for biologists contains articles on many of the points above.

Software and code

Policy information about availability of computer code

Data collection	No original data was collected for this work.
Data analysis	Data analysis used 1. Custom code in MATLAB R2021a, detailed in the manuscript. This included the circlefit function (https://uk.mathworks.com/matlabcentral/fileexchange/5557-circle-fit) 2. PERPL 0.12m (https://bitbucket.org/apcurd/perpl-python3/commits/tag/0.12m) 3. Python library scipy 1.3

For manuscripts utilizing custom algorithms or software that are central to the research but not yet described in published literature, software must be made available to editors and reviewers. We strongly encourage code deposition in a community repository (e.g. GitHub). See the Nature Portfolio guidelines for submitting code & software for further information.

Data

Policy information about availability of data

All manuscripts must include a data availability statement. This statement should provide the following information, where applicable:

- Accession codes, unique identifiers, or web links for publicly available datasets
- A description of any restrictions on data availability
- For clinical datasets or third party data, please ensure that the statement adheres to our policy

The original MINFLUX data (Gwosch et al., 2020) was made available by Stefan Hell. All the re-analyzed data has been deposited to Zenodo at https://doi.org/10.5281/zenodo.5214631.

Human research participants

Policy information about studies involving human research participants and Sex and Gender in Research.

Reporting on sex and gender	No human research participants.
Population characteristics	*Describe the covariate-relevant population characteristics of the human research participants (e.g. age, genotypic information, past and current diagnosis and treatment categories). If you filled out the behavioural & social sciences study design questions and have nothing to add here, write "See above."*
Recruitment	*Describe how participants were recruited. Outline any potential self-selection bias or other biases that may be present and how these are likely to impact results.*
Ethics oversight	*Identify the organization(s) that approved the study protocol.*

Note that full information on the approval of the study protocol must also be provided in the manuscript.

Field-specific reporting

Please select the one below that is the best fit for your research. If you are not sure, read the appropriate sections before making your selection.

☒ Life sciences ☐ Behavioural & social sciences ☐ Ecological, evolutionary & environmental sciences

For a reference copy of the document with all sections, see nature.com/documents/nr-reporting-summary-flat.pdf

Life sciences study design

All studies must disclose on these points even when the disclosure is negative.

Sample size	We re-analyzed all data from every field of view in the nuclear pore complex data of Gwosch et al.. Per-pore analysis (Fig. 1): We chose 20 evident nuclear pore complexes (NPCs) for the per-pore analysis in each dataset of Fig. 1a-e. This is the majority of possible NPCs present in each dataset and allowed assessment of the distributions of NPC diameter and numbers of localizations. Each dataset also included other possible but less clear examples of NPCs, so the actual number of NPCs represented by the original data is unclear. We used both of the two NPCs visible in the original data for Fig. 1f. FOV ensemble analysis (Fig. 2 and Extended Data Fig. 4): We used all localizations in the original NPC data of Gwosch et al.. Localization probability, live-cell results (Extended Data Fig. 3): We used all localizations in the original NPC data of Gwosch et al..
Data exclusions	No data exclusions.
Replication	We re-analyzed existing datasets to assess claims based on those datasets. We ran our analysis code multiple times with the same results.
Randomization	Each dataset that we re-analyzed contained a list of molecular localisation positions acquired under the same experimental conditions. Therefore there was no data for us to randomize. We re-analyzed each dataset independently.
Blinding	We started with the knowledge that data was acquired from NPCs. This allowed both Gwosch et al. and ourselves to interpret and analyze the datasets in comparison with previous NPC data in the literature. Blinding was therefore not useful or needed for this study.

Reporting for specific materials, systems and methods

We require information from authors about some types of materials, experimental systems and methods used in many studies. Here, indicate whether each material, system or method listed is relevant to your study. If you are not sure if a list item applies to your research, read the appropriate section before selecting a response.

Materials & experimental systems

n/a	Involved in the study
☒	☐ Antibodies
☒	☐ Eukaryotic cell lines
☒	☐ Palaeontology and archaeology
☒	☐ Animals and other organisms
☒	☐ Clinical data
☒	☐ Dual use research of concern

Methods

n/a	Involved in the study
☒	☐ ChIP-seq
☒	☐ Flow cytometry
☒	☐ MRI-based neuroimaging